since $(1/\epsilon\epsilon_0)\rho(t)/(\partial\rho(t)/\partial t) \gg 1/e\mu n_0$.

[28]The field at the cathode increases as long as the total space-charge density $\rho\Delta x$ increases. This is assured even though the voltage drop in the space-charge region $[\sim\rho(\Delta x)^2]$ decreases as long as ρ increases more than Δx decreases (see Sec. VI B).

[29]To finally allow for tunneling.

[30]The assumption of surface states for a "pinning of boundary condition" in such materials seems to be misleading.

PHYSICAL REVIEW B VOLUME 7, NUMBER 4 15 FEBRUARY 1973

Resistivity and "One Dimensionality" in Ti_2O_3[†]

L. L. Van Zandt and P. C. Eklund
Department of Physics, Purdue University, Lafayette, Indiana 47907
(Received 6 April 1972)

Energy bands in a Ti_2O_3 lattice are parametrized in terms of overlap matrix elements. The requirements of "one-dimensional" energy bands as an explanation for recently observed specific-heat anomalies are compared to this parametrization and shown to be in conflict by three orders of magnitude. Resistivity measurements on oriented samples are also shown and also fail to support the "one-dimensional" hypothesis.

Sjöstrand and Keesom[1] have recently observed anomalous low-temperature specific heats in samples of Ti_2O_3 doped with a few percent V_2O_3. They tentatively ascribe the anomalous behavior to the presence of holes introduced by the V ions into a "one-dimensional" valence band of the host material with a single low mass direction parallel to the axis. Briefly, the density of electronic states varies in proportion to $E^{1/2}$ in a three-dimensional structure but like $E^{-1/2}$ in a one-dimensional array, where E is the single-electron (or hole) energy as measured from the band edge. The singularity in $E^{-1/2}$ near the band edge provides an enormous density of states for dopant-introduced carriers and so has been proposed to fit the anomalies as observed.

The purpose of this communication is to report resistivity measurements whose interpretation appears to conflict with one dimensionality in the electronic structure and to consider and emphasize the unavoidable implications of one dimensionality, which would suggest that the hypothesis should be accepted only with reluctance.

In considering the implications of the one-dimensional hypothesis, we need to consider the question of the direction of that one dimension, that is, which of the three crystal dimensions is the favored one. Ti_2O_3, with and without vanadium, crystallizes in the corundum structure of symmetry D_{3d}. The structure thus includes a preferred direction, the c axis. To avoid breaking the symmetry, therefore, the favored direction should be the c axis, or there should be three degenerate sets of electronic states with favored directions symmetrically arranged. Both alternatives encounter difficulties when the actual lattice structure is considered, however, as will be seen.

The crystal binding in Ti_2O_3 is strongly ionic in character; three of the 22 electrons of a neutral Ti atom are transferred to oxygen sites, leaving a single d electron on the Ti^{3+} ion. In a rhombohedral field, the five orbital atomic d states are split into two pairs of doubly degenerate e_g states and a single nondegenerate a_{1g} state. That pure Ti_2O_3 is an insulator indicates that the a_{1g} state lies lowest,[3,4] and it is the bands formed from this state that we shall study for one dimensionality.

We shall work in the tight-binding approximation, but since there are several Ti atoms in a unit cell, the calculation is somewhat more complicated than the usual textbook case.

When the atoms are brought together to form molecules, the atomic wave functions overlap and the atomic levels are split into molecular levels. Bringing the molecules together to form a crystal finely splits, or broadens, the molecular levels into bands.

We can simplify somewhat by an approximation in which we treat the individual Ti_2O_3 molecules as identical although in fact there are two sets of molecules related by a glide reflection. The long distance between inequivalent molecules of the same unit cell in the actual structure makes this a slight approximation and one which certainly does not qualitatively change our conclusions.

Ti_2O_3 molecules are located on the vertices of a rhombohedral lattice described by lattice vectors as in Table I, which also relates them to the crystal parameters c and a.

In zeroth order, each Ti site affords one a_{1g} atomic function $\chi_a(\vec{r}-\vec{r}_i)$. The one-electron Hamiltonian is

$$H = -\frac{\hbar^2}{2m}\vec{\nabla}^2 + \sum_i v(\vec{r}-\vec{r}_i)\,, \tag{1}$$

where $\vec{r}_i$ runs over all the Ti ions. We first construct a molecular wave function,

$$\chi_m(\vec{r}) = a_1\chi_a(\vec{r}-\tfrac{1}{2}d\hat{z}) + a_2\chi_a(\vec{r}+\tfrac{1}{2}d\hat{z})\,; \tag{2}$$

TABLE I. Cation locations in TiO_3.

	Molecular separation	Atomic separation in crystal parameters		Atomic separation (in Å)	γ
0	0	$d\hat{z}$	=	2.59	J_0
R_1	a_1 and symmetry-related vectors	$\hat{x}a/\sqrt{3}+\frac{1}{6}z\hat{c}$	=	3.74	$\gamma_1^{(2)}$
		$a_1-\hat{z}d$	=	2.99	$\gamma_1^{(1)}$
		$a_1+\hat{z}d$	=	5.70	$\gamma_1^{(3)}$
R_2	a_1+a_2 and symmetry-related vectors	$\hat{x}a/2\sqrt{3}+\frac{1}{2}\hat{y}a+\frac{1}{2}\hat{z}c$	=	5.44	$\gamma_2^{(2)}$
		$a_1+a_2-\hat{z}d$	=	3.56	$\gamma_2^{(1)}$
		$a_1+a_2+\hat{z}d$	=	7.73	$\gamma_2^{(3)}$
R_3	$\pm(a_1+a_2+a_3)$	$\frac{1}{2}\hat{z}$	=	6.82	$\gamma_3^{(2)}$
		$(a_1+a_2+a_3)-\hat{z}d$	=	4.23	$\gamma_3^{(1)}$
		$(a_1+a_2+a_3)+\hat{z}d$	=	9.41	$\gamma_3^{(3)}$

d is the separation between the two Ti atoms within a molecule. In the representation in which χ_a's are basis functions, the Hamiltonian has the form

$$H=\begin{pmatrix} E_a+\bar{v} & J_0 \\ J_0 & E_a+\bar{v}\end{pmatrix}, \tag{3}$$

in which

$$\bar{v}=\sum_{\vec{r}_i\neq\hat{z}d/2}\int\chi_a^*(\vec{r}-\tfrac{1}{2}\hat{z}d)\,v(\vec{r}-\vec{r}_i)\,\chi_a(\vec{r}-\tfrac{1}{2}\hat{z}d)\,d\vec{r} \tag{4}$$

and

$$J_0=\sum_{\vec{r}_i\neq\hat{z}d/2}\chi_a^*(\vec{r}+\tfrac{1}{2}\hat{z}d)\,v(\vec{r}-\vec{r}_i)\,\chi_a(\vec{r}-\tfrac{1}{2}\hat{z}d)\,d\vec{r}\,. \tag{5}$$

The eigenfunctions of this Hamiltonian are

$$\chi_m^{(\pm)}(\vec{r})=(1/\sqrt{2})\,[\chi_a(\vec{r}-\tfrac{1}{2}\hat{z}d)\pm\chi_a(\vec{r}+\tfrac{1}{2}\hat{z}d)]\,, \tag{6}$$

with energies

$$E_m^{(\pm)}=E_a+\bar{v}\mp J_0\,. \tag{7}$$

The a_{1g} functions χ_a are maximal along the c axis, which connects the nearest-neighbor Ti pairs in the molecule. Hence J_0 should be the largest coupling of all those we discuss.

We now form two bands from the $\chi_m^{(\pm)}(\vec{r})$:

$$\psi_k^{(\pm)}=\frac{1}{\sqrt{N}}\sum_{\vec{R}_j}e^{i\vec{k}\cdot\vec{R}_j}\chi_m^{(\pm)}(\vec{r}-\vec{R}_j)\,. \tag{8}$$

The $\vec{R}_j$ are the lattice vectors of the molecules (see Table I). In standard fashion, taking the bands one at a time, we obtain

$$E_k^{(\pm)}=E_m^{(\pm)}+\sum_{\vec{R}_j\neq0}J_j^{(\pm)}e^{i\vec{k}\cdot\vec{R}_j}\,, \tag{9}$$

where

$$J_j^{(\pm)}=\sum_{\vec{r}_i}{}'\int\chi_m^{*(\pm)}(\vec{r})\,v(\vec{r}-\vec{r}_i)\,\chi_m^{(\pm)}(\vec{r}-\vec{R}_j)\,. \tag{10}$$

The prime on the summation indicates that the $\vec{r}_i$'s do not include the ions of the molecule at $\vec{R}_j=\vec{0}$. The Hamiltonian, however, connects $\chi_m^{(+)}$ and $\chi_m^{(-)}$ states on different molecules. Hence, to find a proper band wave function ψ_k we need to diagonalize

$$H=\begin{pmatrix} E_m^{(+)}+\sum_j e^{i\vec{k}\cdot\vec{R}_j}J_j^{(+)} & \sum_j e^{i\vec{k}\cdot\vec{R}_j}J_j^{(+-)} \\ \sum_j e^{i\vec{k}\cdot\vec{R}_j}J_j^{(-+)} & E_m^{(-)}+\sum_j e^{i\vec{k}\cdot\vec{R}_j}J_j^{(-)}\end{pmatrix}. \tag{11}$$

Each J_j is composed of four parts because there are four atomic wave functions involved. For nearest-neighbor molecules,

$$J_1^{\pm}=\pm\gamma_1^{(1)}+2\gamma_1^{(2)}\pm\gamma_1^{(3)}\,, \tag{12}$$

where

$$\begin{aligned}
\gamma_1^{(1)}&=\frac{1}{2}\int\chi_a^*(\vec{r}-\tfrac{1}{2}d\hat{z})\sum_{r_i}v(\vec{r}-\vec{r}_i)\\
&\qquad\times\chi_a(\vec{r}+\tfrac{1}{2}d\hat{z}-\vec{R}_1)\,d\vec{r}\,,\\
\gamma_1^{(2)}&=\frac{1}{2}\int\chi_a^*(\vec{r}-\tfrac{1}{2}d\hat{z})\sum_{r_i}v(\vec{r}-\vec{r}_i)\\
&\qquad\times\chi_a(\vec{r}-\tfrac{1}{2}d\hat{z}-\vec{R}_1)\,d\vec{r}\,,\\
\gamma_1^{(3)}&=\frac{1}{2}\int\chi_a^*(\vec{r}+\tfrac{1}{2}d\hat{z})\sum_{r_i}v(\vec{r}-\vec{r}_i)\\
&\qquad\times\chi_a(\vec{r}-\tfrac{1}{2}d\hat{z}-\vec{R}_1)\,d\vec{r}\,.
\end{aligned} \tag{13}$$

$\gamma_1^{(1)}$ is an overlap between next-nearest-neighbor Ti ions and is therefore much larger than the other γ's. Similar expressions may be obtained for J_2 and J_3, the only other possibly important molecular overlaps.

Figure 1 indicates the geometry of the couplings, both for J_1^{+} and $J_1^{(+,-)}$. Note that

$$J_j^{\pm}(\vec{R}_j)=J_j^{\pm}(-\vec{R}_j)\,, \tag{14}$$

but that

$$J_j^{(+,-)}(\vec{R}_j)=-J_j^{(+,-)}(-\vec{R}_j)\,. \tag{15}$$

We now perform the sums indicated in Eq. (11) over the $\vec{R}_j$, express the J_j in terms of the γ_j, and expand the resulting sines and cosines in powers of k, the electron-state vector. We then diagonalize the 2×2 determinant for $E_{\vec{k}}$, and near a band edge obtain

$$\begin{aligned}
E_{\vec{k}}=E_a+\bar{v}+6\gamma_1^{(2)}&\pm2(J_0+3\gamma_1^{(1)}+3\gamma_2^{(1)}+\gamma_3^{(1)})\mp\frac{k_x^2+k_y^2}{2}\,a^2\left(\frac{J_0(\gamma_1^{(1)}+\gamma_2^{(1)})}{J_0+3\gamma_1^{(1)}+3\gamma_2^{(1)}+\gamma_3^{(1)}}\pm\gamma_1^{(2)}\right)\\
&\mp\frac{k_z^2c^2}{3}\left(\frac{J_0(\gamma_1^{(1)}+4\gamma_2^{(1)}+3\gamma_3^{(1)})/4+3(\gamma_1^{(1)}+2\gamma_2^{(1)}+\gamma_3^{(1)})^2}{J_0+3\gamma_1^{(1)}+3\gamma_2^{(1)}+\gamma_3^{(1)}}\pm\frac{\gamma_1^{(2)}}{4}\right).
\end{aligned} \tag{16}$$

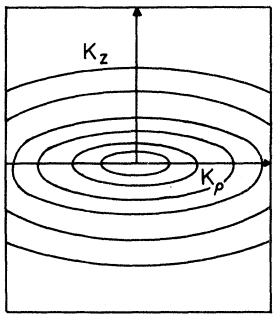

FIG. 1. Cross section of cylindrical Brillouin zone showing cross sections of ellipsoids of constant energy. The three-dimensional zone would be rotationally symmetrical about K_z.

In this expression we have assumed $J_0 \gg \gamma$ and discarded all γ's referring to couplings between sixth-nearest-neighbor Ti atoms and higher. If we further assume, consistently with this picture, that

$$\gamma_1^{(1)} \gg \gamma_2^{(1)}\ ,\ \gamma_3^{(1)}\ ,\ \gamma_1^{(2)}$$

thus near the valence-band edge

$$E_{\vec{k}}^{(+)} \cong E_a + \bar{v} - 6\gamma_1^{(1)} + \tfrac{1}{2}k_\rho^2 a^2 \gamma_1^{(1)} + \tfrac{1}{12}k_z^2 c^2 \gamma_1^{(1)}\ . \tag{17}$$

Naturally, in a three-dimensional crystal, bands can only be one dimensional in some approximate sense. This means the energy structure must be approximately

$$E^{(1)}(k_z) = \hbar^2 k_z^2/2m^*\ . \tag{18}$$

In Ref. 1, good agreement with experimental data was obtained with m^* about two free-electron masses. We can also write this as

$$E_{\vec{k}}^{(1)} = \frac{\hbar^2}{2}\left(\frac{k_z^2}{m_z} + \frac{k_x^2 + k_y^2}{m_\rho}\right)\ , \tag{19}$$

where $m_\rho \gg m_z$, and the relative size of m_ρ is such as to make an unimportant contribution to the energy. Our Eq. (17) is of this form from which we may obtain

$$m_z/m_\rho = 6(a/c)^2 \cong 0.85\ ,$$

since $c/a \cong 2.65$.

The simplest band model thus predicts a slightly greater transverse mass than longitudinal mass. It is also clear from the form of the expressions that the only way to make a significantly larger difference between the two masses is to make $\gamma_3^{(1)} \gg \gamma_1^{(1)}$ and $\gamma_2^{(1)}$.

The experiments[1] can be used to give a lower bound on the mass anisotropy. The data are consistent with the one-dimensionality hypothesis at relative V to Ti concentrations from 10 at.% down at least to 1.5 at.%. The initial slope of the C_v-vs-T curve yields a density of electron states accurately proportional to $n^{-1/2}$ in this range, where n is the relative V concentration.

Let us then consider a Brillouin zone shaped like a right circular cylinder for convenience. The c/a ratio of Ti_2O_3 determines the relative dimensions. Using Eq. (19) for $E(k)$, several isoenergetic surfaces are shown in cross section in Fig. 2(a). As long as the energy surfaces remain ellipsoidal, the density of states is proportional to $E^{1/2}$. When the ellipsoid reaches the zone edge, however, the density-of-states curve changes, and, for energies a few times this initial contact energy, accurately follows an $E^{-1/2}$ dependence. The exact curve of $N(E)$ for this model is shown in Fig. 2(b); $E^{-1/2}$ is also plotted for comparison. To be consistent with the experiments, $N(E)$ must not depart substantially from $E^{-1/2}$ for any of the observed carrier concentrations. Since it was observed that each V ion contributes 0.4 carriers,[1] this means that the $E^{-1/2}$ law must be obeyed for the band 0.6% filled. From these considerations and a little geometry we obtain

$$(m_z/m_\rho)^{1/2} \cong 0.006\,(a/c) \tag{20}$$

or

$$m_\rho = m_z\, 1.95 \times 10^5\ , \tag{21}$$

or m_ρ approximately 5×10^5 free-electron masses.[1] We emphasize that this relative mass disparity is not a consequence of the model or the approximations of tight-binding theory. Within factors of order unity, it is unavoidably demanded by the experiments and the one-dimensional interpretation.

Thus, we need to determine whether the overlap integrals $\gamma_1^{(1)}$ and $\gamma_3^{(1)}$ could conceivably differ by the necessary five orders of magnitude, and thus we require a consideration of the appropriate crystal field d wave functions. There are five such functions $\theta_{2,m}(\theta, \varphi)$, where the polar direction is taken along the c axis. Each Ti ion sits in a site of only C_3 symmetry. Hence, the crystal field can be represented by

$$\begin{aligned} V(\theta, \varphi) = {} & \nu_0\,\theta_{0,0} + \nu_1\,\theta_{1,0} + \nu_2\,\theta_{2,0} \\ & + \nu_3\,\theta_{3,0} + U_3(\theta_{3,3} + \theta_{3,-3}) \\ & + \nu_4\,\theta_{4,0} + U_4(\theta_{4,3} + \theta_{4,-3}) \quad + \cdots\ . \end{aligned} \tag{22}$$

Higher-order terms in $V(\theta, \varphi)$ do not mix d states. Thus the one-electron Hamiltonian at the Ti ion must be of the form

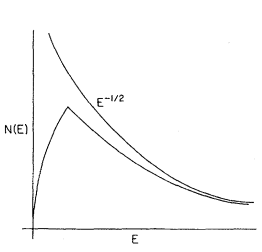

FIG. 2. Density of electron states as a function of electron energy for the structure shown in Fig. 1. The cusp occurs when the isoenergetic ellipsoid just touches the walls of the zone. $E^{-1/2}$ is shown for comparison, normalized at large E.

$$\begin{matrix} \theta_{2,2} & f_2 & 0 & 0 & a & 0 \\ \theta_{2,1} & 0 & f_1 & 0 & 0 & a \\ \theta_{2,0} & 0 & 0 & f_0 & 0 & 0 \\ \theta_{2,-1} & a & 0 & 0 & f_1 & 0 \\ \theta_{2,-2} & 0 & a & 0 & 0 & f_2 \end{matrix} . \qquad (23)$$

The eigenfunctions are therefore

$$\begin{cases} a_1\theta_{2,2}+b_1\theta_{2,-1} \\ a_1\theta_{2,-2}+b_1\theta_{2,1} \end{cases}$$

$$\begin{cases} a_1\theta_{2,-1}-b_1\theta_{2,2} \\ a_1\theta_{2,1}-b_1\theta_{2,-2} \end{cases} \qquad (24)$$

$$\theta_{2,0} \ ;$$

the brackets indicate degeneracy.

Since Ti_2O_3 is an insulator, the lowest-lying state must be

$$\theta_{2,0}=3z^2-r^2 . \qquad (25)$$

This attains a maximum value of 2 along the z direction, which favors $\gamma_3^{(1)}$ compared to $\gamma_1^{(1)}$. Along the direction of second-nearest-neighbor Ti, however, its value is about -0.8 which is still of the same order of magnitude. Thus tight-binding theory is unable *by five orders of magnitude* to yield the necessary mass anisotropy to make the one-dimensional hypothesis convincing.

Our discussion has neglected the hybridization between Ti d orbitals and O $2p$ orbitals and the resulting superexchange enhancement of the coupling. However, examination of the lattice shows that oxygen ions are favorably placed for the enhancement

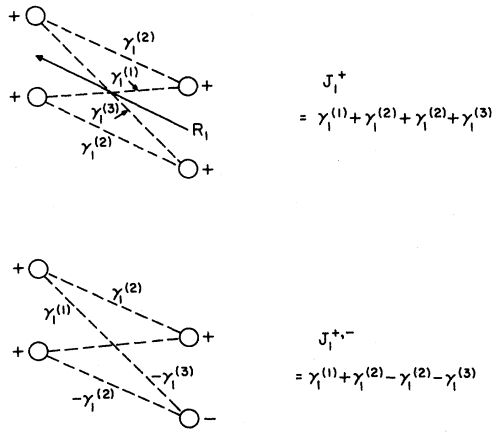

FIG. 3. Description of interionic overlaps used in calculating energy-band parameters J. + and − signs near a metal ion indicate the relative signs of χ_a centered on that ion used in forming χ_m. Dotted lines link sites of overlapping χ_a's entering the integral for the respective γ's.

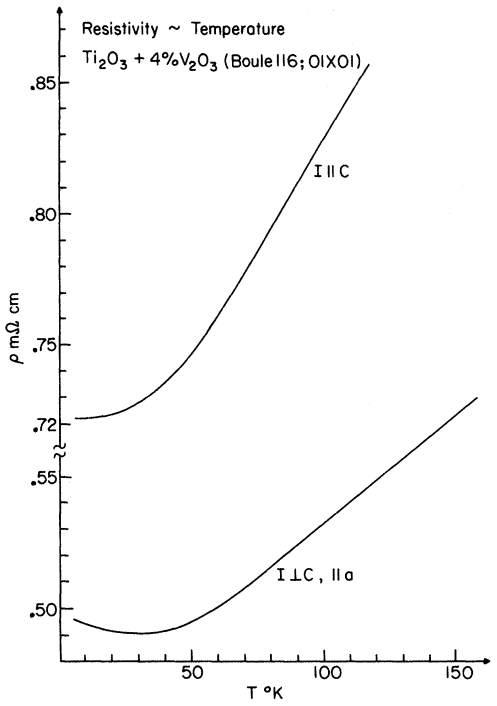

FIG. 4. Resistivity as a function of temperature for $Ti_{0.96}V_{0.04}O_3$ for current parallel and perpendicular to the c axis.

of $\gamma_1^{(1)}$, $\gamma_1^{(2)}$, and $\gamma_2^{(1)}$, but not for $\gamma_1^{(3)}$. Thus the inclusion of superexchange in our considerations would not help.

Sjöstrand and Keesom[1] have called attention to the theory of Labbé and Friedel,[5] which similarly employs a one-dimensional band structure to explain properties of V_3Si and related compounds of the β-tungsten structure. It is interesting to contrast these two compounds to see why the one-dimensional hypothesis does not encounter similar difficulties in V_3Si.

The large overlap favoring one dimensionality is between nearest-neighbor V ions in V_3Si and competes with overlaps between second nearest neighbors about 15% further removed. By contrast, in Ti_2O_3 the principal overlap must be between *fifth*-nearest neighbors and competes with a second-nearest neighbor about 30% *closer*. Second, the specific-heat anomalies in V_3Si are substantially smaller than those observed in Ti_2O_3. The necessary mass anisotropy for satisfactory one dimensionality is correspondingly greatly reduced. Finally, the specific-heat anomaly in V_3Si arises from contributions from three degenerate bands, whereas in Ti_2O_3, the entire anomaly must be due, for symmetry reasons, to a single band.

Since V_3Si is a cubic crystal, the resistivity is necessarily isotropic. In Ti_2O_3, however, the resistivity should not be isotropic. Indeed, since

there is only one, rather than three, mutually perpendicular one-dimensional bands, the resistivity should be highly anisotropic. Magnetoresistance and Hall effect in oriented samples of V-doped Ti_2O_3 were measured by Honig and collaborators.[6] Data from these experiments established that conduction was by holes in the low-lying a_{1g} band we have been discussing, but the huge anisotropy the one-dimensional model predicts was not observed. However, since only a very few of the data points in in Ref. 5 bear on this question, we measured the resistivity as a function of temperature for two oriented samples taken from adjacent slices of the boules used by Sjöstrand and Keesom. The data are plotted in Fig. 3. Measurements were made by a standard four-probe technique described in Ref. 5.

Some anisotropy is observed, as is virtually inevitable in this low-symmetry system, but only about 50%; more important, note that the resistivity is *higher* in the c-axis direction than in the basal plane. The resistivity measurements are totally inconsistent with the one-dimensional interpretation of the specific-heat anomalies.

ACKNOWLEDGMENTS

The authors are grateful to M. E. Sjöstrand and P. H. Keesom for valuable discussions of these topics and other as yet unpublished data.

†Work supported by the Advanced Research Projects Agency (IDL Program No. DAHC-0213) and the National Science Foundation (MRL Program No. GH 33574).

[1]M. E. Sjöstrand and P. H. Keesom, Phys. Rev. Lett. **27**, 1434 (1971); and unpublished.

[2]Approximately $E^{-1/2}$ density of states behavior can arise in three dimensional systems as well, and can be associated with a supression of zero, one, or two translational degrees of freedom of the electron. [P. C. Eklund & L. L. Van Zandt, Phys. Lett. A (to be published)].

[3]L. L. Van Zandt, J. M. Honig, and J. B. Goodenough, J. Appl. Phys. **39**, 594 (1968).

[4]W. H. Kleiner, MIT Lincoln Laboratory Solid State Research Report No. 3, 1967 (unpublished).

[5]J. Labbé and J. Friedel, J. Phys. (Paris) **27**, 153 (1966).

[6]J. M. Honig, L. L. Van Zandt, T. B. Reed, and J. Sohn, Phys. Rev. **182**, 863 (1969).

PHYSICAL REVIEW B VOLUME 7, NUMBER 4 15 FEBRUARY 1973

Collision-Induced Nonlinear Excitations

L. Stenflo and M. Y. Yu*
Department of Plasma Physics, Umeå University, 901 87 *Umeå, Sweden*
(Received 7 February 1972)

We demonstrate that a velocity-dependent collision frequency can introduce significant nonlinearities in the theory of a homogeneous, unmagnetized plasma. By means of a practical collision model which allows us to obtain useful information on nonlinear plasma phenomena without involving the mathematical complexity usually associated with collision operators, we investigate the problems of self-focusing, parametric excitation, and third-order frequency mixing. Our results are compared with those of previous authors. It is shown that the collision-induced nonlinear excitations considered here may be more important than those due to other mechanisms.

I. INTRODUCTION

Model collision operators with velocity-independent collision frequencies are often used to consider the effect of collisions on plasma waves. Since, in reality, particles with high and low velocities have quite distinct collision characteristics, the use of these models cannot generally be justified, except perhaps for a few cases in which the exact form of the collision frequency happens to be unimportant. It is therefore necessary to use more realistic, but often mathematically complicated, collision models, such as the full Boltzmann or Fokker–Planck operators. In considering linear problems, one may still occasionally obtain solutions to these complicated kinetic equations by employing some sort of perturbation or numerical techniques. However, it would be impractical, in general, to use the latter equations in considering nonlinear problems.

In this paper, we consider collisional wave excitation in a spatially uniform plasma by using a fairly realistic, yet simple, collision model. In fact, we use the Lorentz collision operator[1] with the velocity-dependent collision frequency represented by the so-called Harp model.[2] This model, which will be discussed in Sec. II, assumes that electrons with energy less than a certain fixed value experience no collisions, while those with higher energy suffer an infinite number of colli-